

Mathematical Modeling on Dynamic Characteristics of the Breakdown Process in Narrow-Gap of SF₆ Based on the FCT Algorithm

Qiuping Zheng¹, Dianchun Zheng²

¹Instrumentation Technology & Economy Institute, Beijing, China

²Harbin University of Science and Technology, Harbin, China

Email: zhengqiupingnicole@hotmail.com, zhengdianchun@126.com

How to cite this paper: Zheng, Q.P. and Zheng, D.C. (2019) Mathematical Modeling on Dynamic Characteristics of the Breakdown Process in Narrow-Gap of SF₆ Based on the FCT Algorithm. *Applied Mathematics*, 10, 769-783.

<https://doi.org/10.4236/am.2019.109055>

Received: August 21, 2019

Accepted: September 23, 2019

Published: September 26, 2019

Copyright © 2019 by author(s) and Scientific Research Publishing Inc.

This work is licensed under the Creative Commons Attribution International License (CC BY 4.0).

<http://creativecommons.org/licenses/by/4.0/>



Open Access

Abstract

The two-dimensional and self-consistent fluid model of the SF₆ discharge was established based on the electron and ions continuity transfer equations coupled to Poisson's equation, and also simultaneously considered the photoionization event, and then the flux corrected transport technique (FCT) was employed to numerically solve the particle flux-continuity equations, and some significant microphenomena were achieved that the dynamic behaviors of the charged particles, the spatio-temporal evolution of the discharge channel and the transformation law of the avalanche-streamer for the SF₆ narrow-gap were revealed in this paper.

Keywords

FCT, SF₆, Avalanche, Streamer, Photoionization

1. Introduction

Usually, the approaches to explore gas discharge phenomenon can be classified into experimental and theoretical methods. Experimental method can directly observe the discharge events, but the discharge mechanisms have not been clearly discovered in detail. However, the theoretical method not only gains key data for the dielectric breakdown of gases, but also some microcosmic parameters on controlling dynamic behaviors of charged particles produced in the time of the gas discharge process are founded [1] [2] [3]. Recently, the computational fluid dynamics has been widely used in the gas discharge field due to its advantages in explicit physical concept, legible image exhibition and highly calculating efficiency [4] [5] [6].

Despite the fact that the electron and ion densities can attain very steep gradients and make the shock fronts in particulate fluids along the discharge channel when the gas discharge is triggered and developed in the overall process under the stimulation of electric field, the FCT technique (flux corrected transport) shows high efficiency and accuracy dealing with the intricacy situation [7] [8] [9]. By virtue of the excellent thermodynamic, dielectric and transport properties, SF₆ is widely used in the electrical industry, especially in the high voltage circuit breaker technology, although it might be replaced by the environment friendly insulating gases. Nevertheless, it is necessary to accurately find microcosmic mechanisms of the particle dynamical behaviors, the spatio-temporal characteristics of the electric field and the track evolution of the discharge channel along the direction of the specific discharge development for broader application domain.

This paper is organized as following: the mathematical model, the FCT algorithm and constraint conditions are carefully presented in Section 2, and the results of the mathematical simulation are analyzed in Section 3 including the following contents: 3.1, avalanche phase; 3.2, streamer formation phase; 3.3, the discharge channel evolution and the photoionization effect. Some valuable conclusions are given in Section 4.

2. The Model and FCT Algorithm

2.1. Model of the Gas Discharge

The model for the narrow-gap with parallel plate electrodes which are filled with SF₆ gas has been presented in detail [10] [11], and the spatio-temporal evolution of the SF₆ discharge overall process is mathematically modeled by a set of equations governing the transport of particles, moment and energy for ions and electrons together with the electric field equation as follows [12] [13]:

$$\frac{\partial(N_e)}{\partial t} = S_{ph} + N_e\alpha|v_e| - N_e\eta|v_e| - N_eN_p\beta - \frac{\partial(N_e v_e)}{\partial z} + \frac{\partial}{\partial z} D \frac{\partial N_e}{\partial z} \quad (1)$$

$$\frac{\partial(N_p)}{\partial t} = S_{ph} + N_e\alpha|v_e| - N_eN_p\beta - N_nN_p\beta - \frac{\partial(N_p v_p)}{\partial z} \quad (2)$$

$$\frac{\partial(N_n)}{\partial t} = N_e\eta|v_e| - N_pN_n\beta - \frac{\partial(N_n v_n)}{\partial z} \quad (3)$$

here t is the time, r and z are the radius and axis distances for the calculating subregion; N_e , N_p and N_n are the electron, positive and negative ion densities; v_e , v_p and v_n are respectively the electron, positive and negative ion drift velocity; the symbols α , β , η and D are ionization, adsorption, recombination coefficient and electron diffusion coefficient, respectively, their values have been taken from reference literature [14], and the S_{ph} is photoionization source term. Collision ionization process between electrons and neutral particles at atmospheric pressure radiate photons, and these photons are absorbed by molecules according to a certain probability, in this situation, once photon energy

reaches the ionization critical value, then the photoionization process occurs and produces a certain amount of the photo electron. Generally speaking, the number of photon electron is much smaller than that of the electrons generated by impact ionization. However, these photon electrons would result in the formation of the secondary avalanche, which moves towards the head of the first avalanche, composes a big avalanche and accelerates the development of the discharge process. Hence the photoionization effect plays a significant role in the gas discharge process. The term S_{ph} , being a source term due to photoionization, is represented as shown below:

$$S_{ph}(z) = \gamma_p \int_0^d \Omega(z-z') N_e(z') \alpha^*(z') |v_e(z')| \times \exp(-\mu|z-z'|) dz' \quad (4)$$

here γ_p , α^* and μ are second ionization, excitation and absorption coefficients, and Ω is the solid angle subtended at z' by the disk charge at the point z . A detail solution about S_{ph} can be referred to the literature [15].

Taking into account the distortion of space charge effects on the electric field, the Poisson equation is given by:

$$\nabla^2 \varphi = \frac{\partial^2 \varphi}{\partial r^2} + \frac{1}{r} \frac{\partial \varphi}{\partial r} + \frac{\partial^2 \varphi}{\partial z^2} = -\frac{q}{\varepsilon_0} (N_p - N_e - N_n) \quad (5)$$

where φ is the electric potential; q is the electronic charge; ε_0 is the permittivity of the free space. The current I in the external circuit due to the motion of electrons and ions between the electrodes is calculated by the Sato formula [16]:

$$I = \frac{\pi r^2 q}{d} \int_0^d (N_p v_p - N_n v_n - N_e v_e) dz \quad (6)$$

here, r is the radius of the discharge channel, q is the electronic charge.

The convection term of particle's continuity Equations (1)-(3) are solved by the FCT technique and other items are used the finite difference directly to solve and the Poisson's Equation (5) is numerically resolved by the over-relaxation iteration.

2.2. FCT Algorithm

The convective terms of Equations (1), (2) and (3) are written as

$$\left. \frac{\partial N}{\partial t} \right|_{\text{conv}} = -\frac{\partial(Nv)}{\partial x}, \text{ where symbol } N \text{ shows the density of the particle species}$$

and v is their velocities.

Taking (rN) as the dependent variable for an axisymmetric cylindrical coordinate system, then

$$\left. \frac{\partial(rN)}{\partial t} \right|_{\text{conv}} = -\frac{\partial f}{\partial r} - \frac{\partial g}{\partial z} \quad (7)$$

where

$$f = rNv_r, g = rNv_z \quad (8)$$

The flux corrected transport algorithm is as follows [17]:

1). Compute $F_{i+\frac{1}{2},j}^L$ and $G_{i,j+\frac{1}{2}}^L$ by a low order monotonic scheme (donor cell).

2). Compute $F_{i+\frac{1}{2},j}^H$ and $G_{i,j+\frac{1}{2}}^H$ by a high order scheme.

3). Define the anti-diffusive fluxes:

$$A_{i+\frac{1}{2},j} = F_{i+\frac{1}{2},j}^H - F_{i+\frac{1}{2},j}^L, \quad A_{i,j+\frac{1}{2}} = G_{i,j+\frac{1}{2}}^H - G_{i,j+\frac{1}{2}}^L \tag{9}$$

4). Compute the low order time advanced solution:

$$N_{i,j}^{td} = N_{i,j}^t - \frac{1}{\Delta V_{i,j}} \left(F_{i+\frac{1}{2},j}^L - F_{i-\frac{1}{2},j}^L + G_{i,j+\frac{1}{2}}^L - G_{i,j-\frac{1}{2}}^L \right) \tag{10}$$

5). Limit the anti-diffusive fluxes:

$$A_{i+\frac{1}{2},j}^C = A_{i+\frac{1}{2},j} C_{i+\frac{1}{2},j}, \quad 0 \leq C_{i+\frac{1}{2},j} \leq 1 \tag{11}$$

$$A_{i,j+\frac{1}{2}}^C = A_{i,j+\frac{1}{2}} C_{i,j+\frac{1}{2}}, \quad 0 \leq C_{i,j+\frac{1}{2}} \leq 1 \tag{12}$$

6). Apply the limited anti-diffusive fluxes:

$$N_{i,j}^{t+\Delta t} = N_{i,j}^{td} - \frac{1}{\Delta V_{i,j}} \left(A_{i+\frac{1}{2},j}^C - A_{i-\frac{1}{2},j}^C + A_{i,j+\frac{1}{2}}^C - A_{i,j-\frac{1}{2}}^C \right) \tag{13}$$

where $V_{i,j}$, $r_{i,j}$, $N_{i,j}$ and $C_{i,j}$ are the volume, radial distance, density and anti-diffusive coefficient of the (i, j) cell, and further details and calculation procedure on the FCT can be found in the literature [3].

2.3. Constraint Conditions

In this paper, schematic diagram and the constraint conditions for parallel-plate electrodes discharge under atmospheric pressure are set as shown in **Figure 1**, and the calculation model is converted to a two-dimensional structure by rotating the axis of symmetry. In the present study, the gap distance between the electrodes filled with SF_6 gas is 5 mm under the pressure 0.1 MPa and temperature

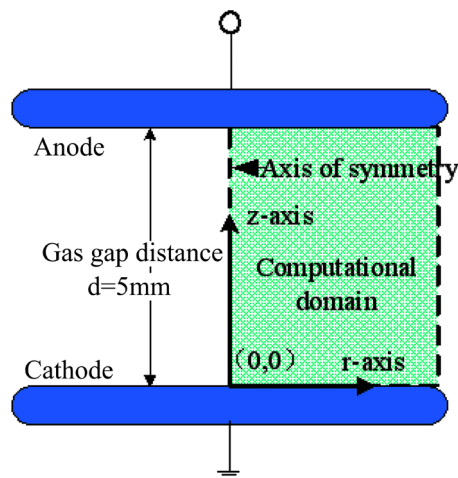


Figure 1. Schematic diagram of mathematical modeling.

300 K. The spatial mesh chosen to be uniform with 40,000 mesh points, namely, the longitudinal axis (z -axis) and the radial axis (r -axis) are all uniformly divided into 200 grids. Then $\Delta t = 0.05 \times 10^{-9}$ s is taken as time step, which is significantly smaller than that required for stability of the used numerical scheme [3]. At the initial moment of time for gas discharge, the quasi-neutral plasma spot of Gaussian shape in the radial and axial directions is placed at the front of cathode:

$$n_e|_{t=0} = n_p|_{t=0} = n_0 \exp \left[-\left(\frac{r}{\delta_r}\right)^2 - \left(\frac{z-z_0}{\delta_z}\right)^2 \right] \quad (14)$$

where r, z is the radial and axial coordinates respectively; the origin of coordinates ($r = z = 0$) is positioned at the center of cathode surface, the peak value density of particles (seed electrons and positive ions) is $n_0 = 10^6 \text{ m}^{-3}$, the position of initial plasma $z_0 = 0.1 \text{ cm}$, characteristic scales $\delta_r = 2.5 \times 10^{-4} \text{ m}$ and $\delta_z = 2.5 \times 10^{-4} \text{ m}$.

Boundary conditions for electrons and positive ions at the electrodes are as follows:

$$\left. \frac{\partial n_e}{\partial z} \right|_{z=0} = \left. \frac{\partial n_e}{\partial z} \right|_{z=d} = 0, \quad \left. \frac{\partial n_p}{\partial z} \right|_{z=0} = \left. \frac{\partial n_p}{\partial z} \right|_{z=d} = 0$$

The solution of Poisson's equation is subject to the following boundary conditions:

$$V|_{z=0} = V_0, \quad V|_{z=d} = 0, \quad \left. \frac{\partial V}{\partial r} \right|_{r=0} = 0, \quad V|_{r=R} = V_0 \frac{z}{d}$$

where V_0 is the applied voltage, r is the radius of the computational domain.

3. Modeling Results

The space between parallel-plane electrodes 0.5 cm apart is filled SF₆ gas with standard atmospheric pressure and commercial purity, and the 46 kV DC is applied on the anode plane, then the cathode grounding. The incepting discharge of the model is triggered by the seed electrons having a Gaussian distribution near the cathode at $t = 0$ ns (located at 0.1 cm from the cathode as mentioned earlier). Under the electric field, the seed electrons obtain energy to migrate, impact the neutral molecules and produce much more charged particles, so that the current through parallel-plane electrodes is shown in **Figure 2**. The transition time of the electron for the model is about 10 ns, according to the principle of gas discharge, the whole discharge process undergoes two phases from the avalanche to the streamer phase while the discharge incepted.

3.1. Avalanche Phase

The electric field stress 92 kV/cm applied to the SF₆ gap, which slightly larger than the threshold value 89.6 kV/cm, easily renders the discharge happen smooth-

ly. With the electrons migrating to the anode and impacting with neutral molecules, an electron swarm is quickly made up as shown in **Figure 3**. When about 7.7 ns moment, the peak value of the electron swarm is up to the $1.01 \times 10^{18} \text{ cm}^{-3}$ at the point $z = 0.25 \text{ cm}$ apart from the cathode, and corresponding positive and negative ions densities are $3.97 \times 10^{18} \text{ cm}^{-3}$ and $3.22 \times 10^{18} \text{ cm}^{-3}$ respectively as shown in **Figure 7** and **Figure 8**, then the distortion of the space electric field is not remarkable as shown in **Figure 4** at 7.5 and 7.7 ns moments, therefore the interval from $t = 0 \text{ ns}$ to the $t = 7.7 \text{ ns}$ usually is known as the avalanche phase according to the gas discharge theory [18].

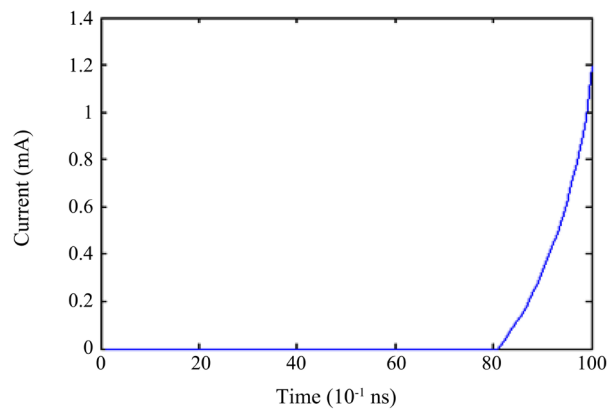
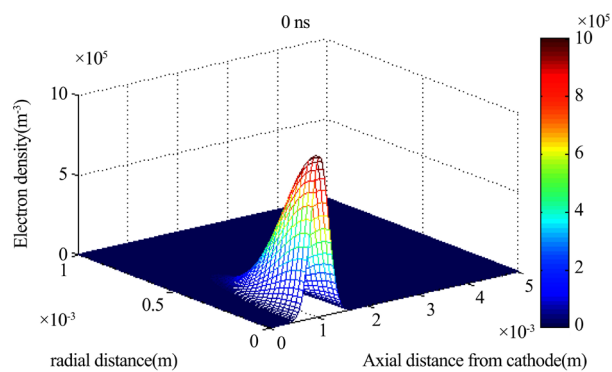
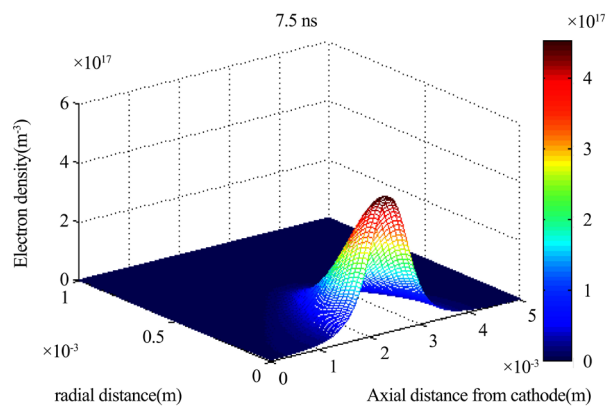


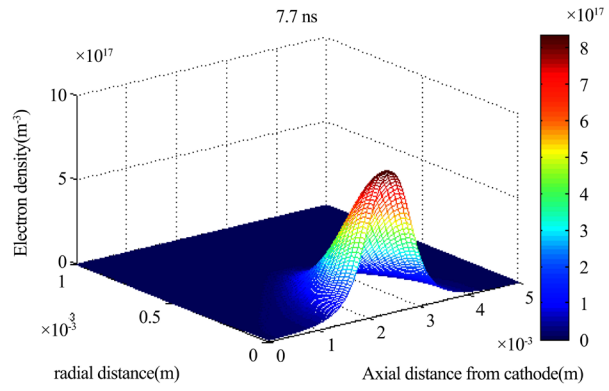
Figure 2. External circuit current.



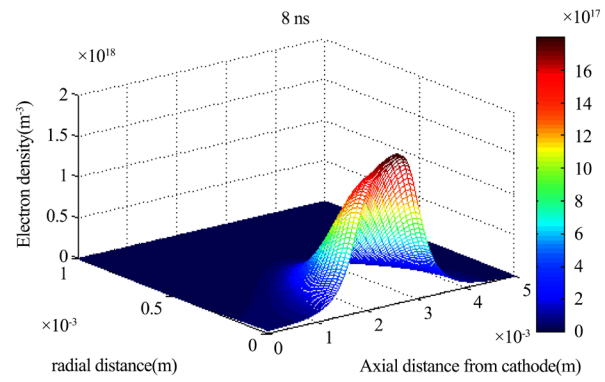
(a) Electron density at 0 ns



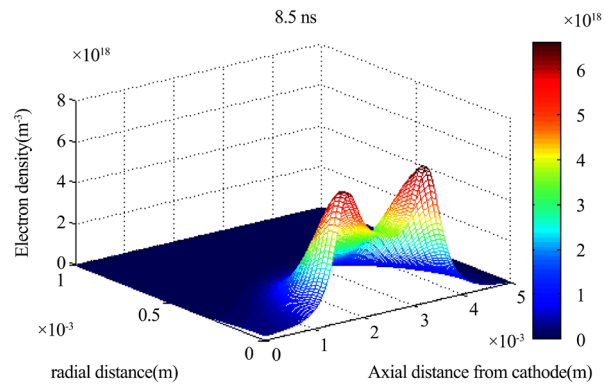
(b) Electron density at 7.5 ns



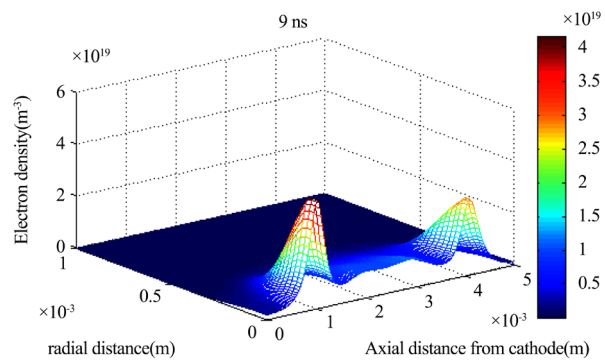
(c) Electron density at 7.7 ns



(d) Electron density at 8.0 ns

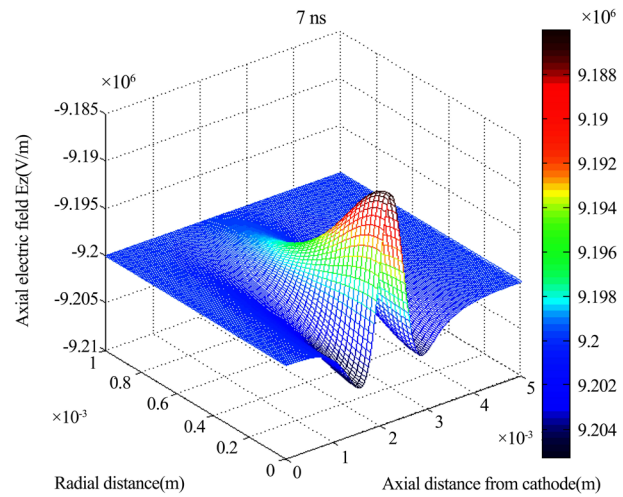


(e) Electron density at 8.5 ns

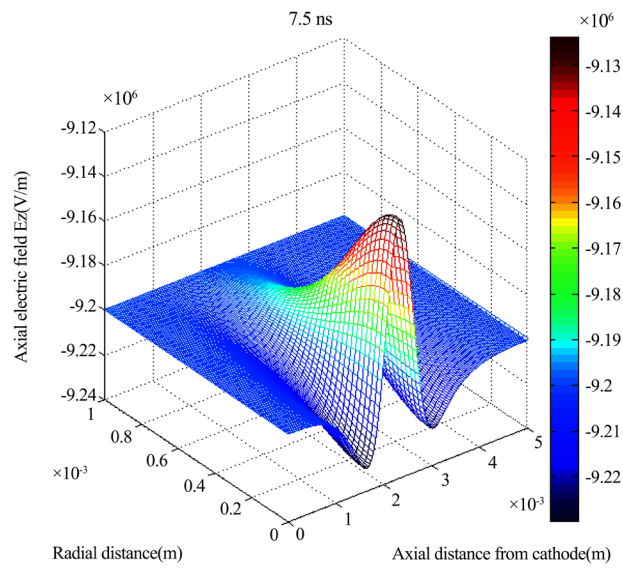


(f) Electron density at 9.0 ns

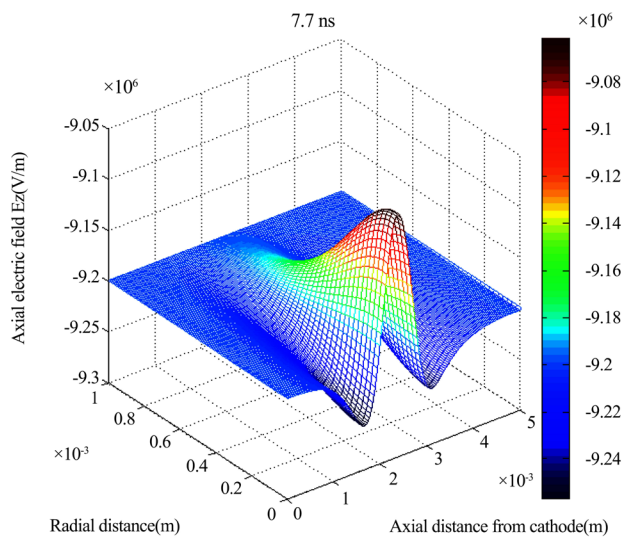
Figure 3. Electron densities at 0 ns, 7.5 ns, 7.7 ns, 8.0 ns, 8.5 ns and 9.0 ns, respectively.



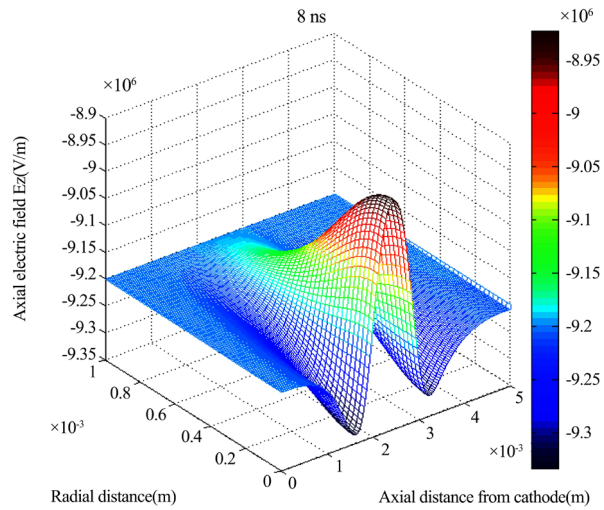
(a) Axial electric field at 7.0 ns



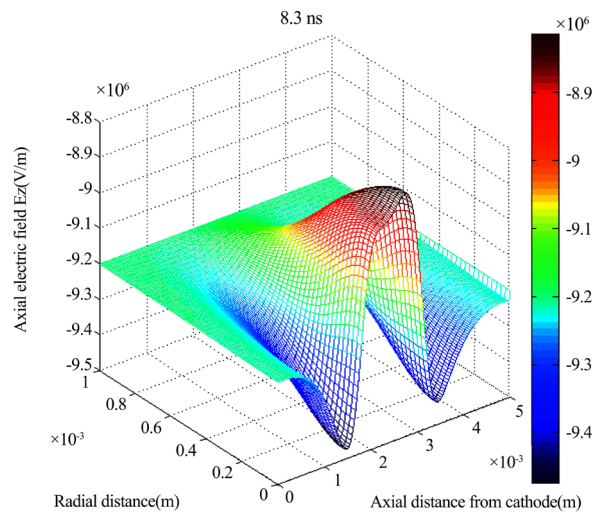
(b) Axial electric field at 7.5 ns



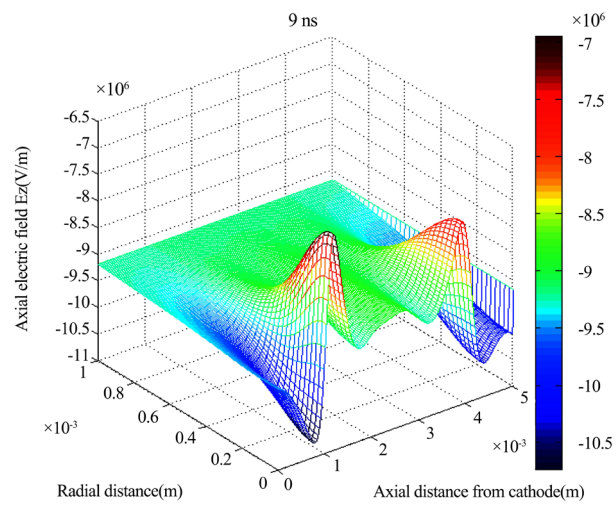
(c) Axial electric field at 7.7 ns



(d) Axial electric field at 8.0 ns



(e) Axial electric field at 8.3 ns



(f) Axial electric field at 9.0 ns

Figure 4. Axial electric fields for SF6 gas at 7.0 ns, 7.5 ns, 7.7 ns, 8.0 ns, 8.3 ns and 9.0 ns, respectively.

3.2. Streamer Phase

When the avalanche volume reaches to the critical value, it instantly changes the avalanche phase into the streamer phase, namely, the streamer phase formation [19] [20]. It is demonstrated in **Figure 3** and **Figure 4** that the electron densities are visibly larger than that of the avalanche phase in the interval 7.7 - 8.0 ns, although the distorting of space electric field is still slight enhancement, it is considered an initial period of the streamer phase.

From the 8.0 ns moment, the streamer discharge is rapidly development, its volume is promptly expanded and the length is also stretched quickly, and simultaneously the electric field distortion is also exacerbated as shown in **Figure 5**, then the mainly changes of the density distribution of charged particles for the electron, positive and negative ions on the axial direction are shown in **Figures 6-8**, the procedure described is rather intricacy including the dynamical behaviors of the charged particles in the electric field [21] [22].

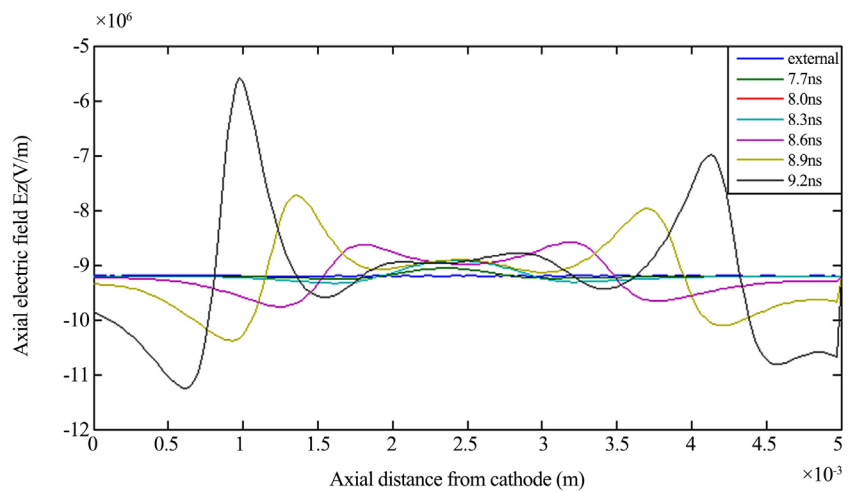


Figure 5. Axial electric field distributions at 7.7 ns, 8.0 ns, 8.3 ns, 8.6 ns, 8.9 ns and 9.2 ns, respectively.

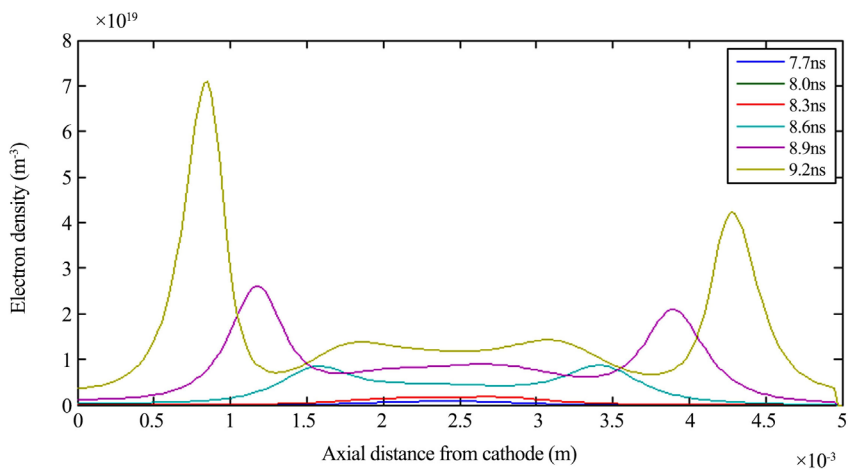


Figure 6. Axial electron distributions at 7.7 ns, 8.0 ns, 8.3 ns, 8.6 ns, 8.9 ns and 9.2 ns, respectively.

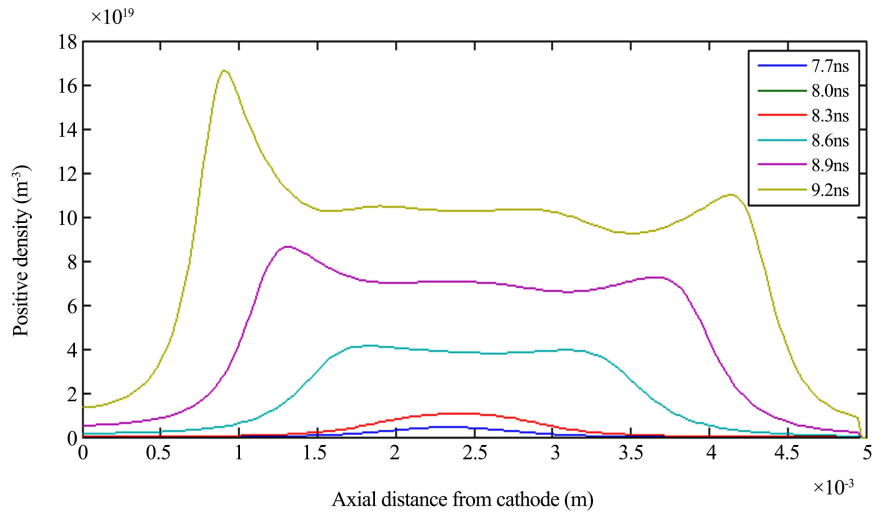


Figure 7. Axial distributions of positive ions at 7.7 ns, 8.0 ns, 8.3 ns, 8.6 ns, 8.9 ns and 9.2 ns, respectively.

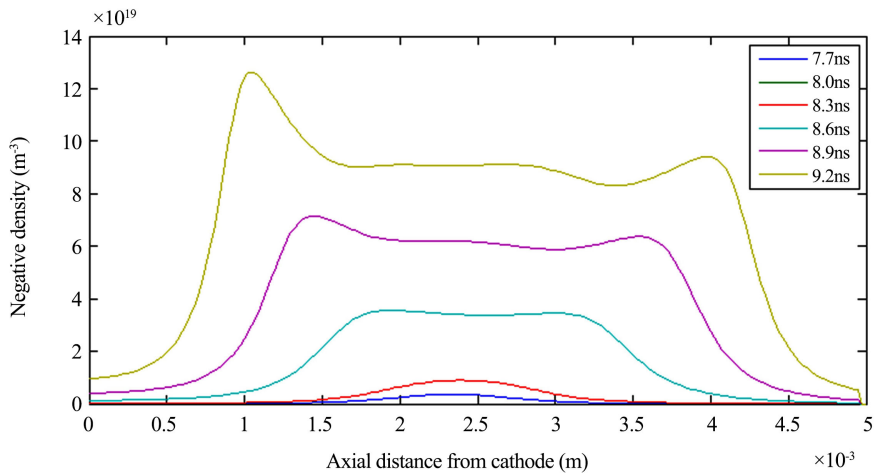


Figure 8. Axial distributions of negative ions at 7.7 ns, 8.0 ns, 8.3 ns, 8.6 ns, 8.9 ns and 9.2 ns, respectively.

1) The anode-directed streamer

When the transformation avalanche into the streamer phase, the peak value of the electron densities from location $z = 0.25$ cm at 7.7 ns to the point $z = 0.44$ cm at $t = 9.2$ ns is shown in **Figure 6**, and the streamer head moves to the anode at an average speed 1.33×10^6 cm/s. The positive and negative ion densities in the anode-directed streamer head increase steadily from $4.43 \times 10^{18} \text{ cm}^{-3}$ to $1.09 \times 10^{19} \text{ cm}^{-3}$ and from $3.62 \times 10^{18} \text{ cm}^{-3}$ to $9.41 \times 10^{19} \text{ cm}^{-3}$ respectively shown in **Figure 7** and **Figure 8**. The head of the anode-directed streamer shows the electro-negativity due to gathering most electrons and greatly enhanced field intensity of the short distance between the head with the anode plate, so that SF_6 molecule ionization in this small region is dramatically aggravated, and many more electrons are reproduced and the head radius continuously becomes bigger and bigger, the iterative process finally ends

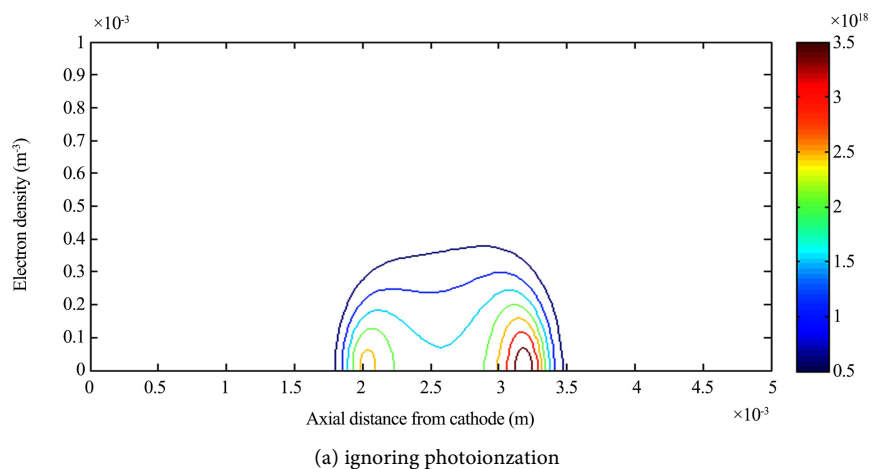
until the head arrives at the anode plate.

2) The cathode-directed streamer

As shown in **Figure 6**, the curve of electron distribution at $z = 0.18$ cm and $t = 8.3$ ns presents the clearly escalating trend, that is to say, the event of the cathode-directed streamer obviously happens, then the appeared moment of the cathode-directed streamer is later than that of the anode-directed one. In contrast with anode-directed streamer, the head of the cathode-directed streamer presents the electro-positivity, because the electric field is strengthened in the short space between the cathode plate and the head, then the ionization rate of the SF_6 molecule is greatly accelerated and much stronger, the velocity of the cathode-directed streamer at 9.2 ns is 0.92×10^6 cm/s at $z = 0.088$ cm location, which is only about 70% of the velocity of the anode-directed streamer in the same moment.

3.3. Discharge Channel and Photoionization

As mentioned above, the discharge process in the narrow-gap of the SF_6 undergoes transformation from the avalanche to the streamer phase, once the streamer is triggered it soon develops respectively towards the anode and cathode plate, namely, the anode-directed streamer and the cathode-directed streamer, at the same time accompanied by the photoionization appeared, the streamer volume not only grows quickly presenting a near cylindrical shape and but also the streamer length becomes much longer till through the anode and cathode plate, then the discharge path of the both electrode is formed and known as a breakdown channel. The fact has been proved by the experiment results and theoretical demonstration, the photoionization plays an important role and not been overlook when the whole discharge process in the narrow-gap of the SF_6 undergoes transformation from the avalanche to the streamer phase. The results of the mathematical modeling in this paper shows in **Figure 9**, considering and ignoring photoionization could achieve different results, if you ignore the photoionization effect, you might get the false result [23].



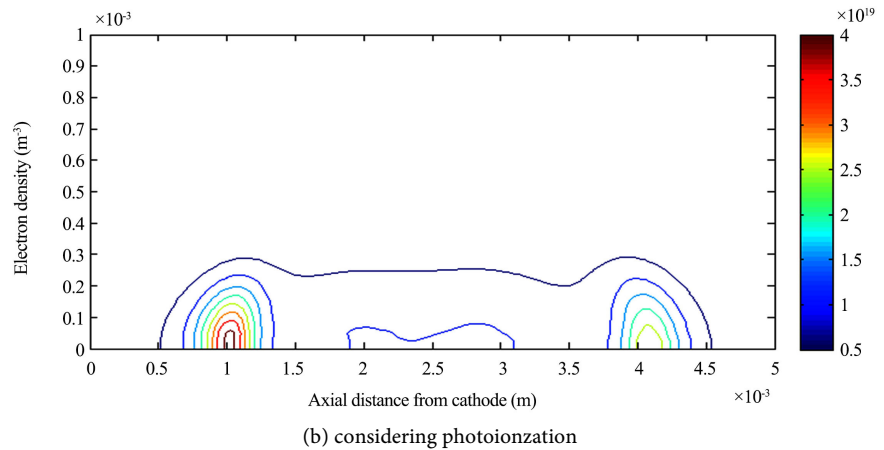


Figure 9. Electron density contour in SF₆ at 9 ns.

4. Conclusions

Based on the fluid model of gas discharge and the FCT algorithm, dynamic characteristics of the SF₆ breakdown process in narrow-gap has mathematically modeled and some important facts has demonstrated that the FCT algorithm is an efficient theoretical way to deal with the troublesome problems having shock fronts in the discharge channel. The results are both shown via easy visualization for the complicated course of the SF₆ discharge and revealed dynamic characteristics of the charged particles during the SF₆ discharge process in narrow-gap.

According to the mathematical model and numerical analysis results in this paper, the breakdown process in narrow-gap of SF₆ still presents two phases at the standard atmospheric pressure, and parallel-plane electrodes 0.5 cm apart and the 46 kV DC applied. Moreover, some facts are indicated that when electrons increase to a certain amount and the avalanche phase changes into the streamer phase. On the one hand, in the electron avalanche phase, the collision ionization is the key rule for producing electrons and making them grow fast until the electron swarms up to the $1.01 \times 10^{18} \text{ cm}^{-3}$. The microcosmic mechanisms of the particle dynamical behaviors, the spatio-temporal characteristics of the electric field and the track evolution of the discharge channel are shown in **Figure 3** and **Figure 4** in the interval from $t = 0 \text{ ns}$ to the $t = 7.7 \text{ ns}$. In this interval, the collision between SF₆ molecule and seed electrons is only triggered by the external electric field. When time ranges from $t = 7.7 \text{ ns}$ to the 8.0 ns, a dramatic change happens in the electron number and electric field of the gas-gap; that is to say, the streamer discharge would be coming. On the other hand, in the streamer phase, from the 8.0 ns moment, the streamer discharge is rapidly developing; its volume is promptly expanded and the length is also stretched quickly, and simultaneously the electric field distortion is also exacerbated as shown in **Figure 5**, then the main changes of the density distribution of charged particles for the electron, and positive and negative ions on the axial direction are shown in **Figures 6-8**.

In a nutshell, the photoionization effect plays a pivotal role in the process of

the streamer discharge phase.

Accompanied by the photoionization, the space charges of the gas-gap are multiplicatively increased and led to extremely distorting of the electric field within the discharge channel, and then the streamer dramatically develops toward both anode and cathode plates, and a plasma region is left in the central part of the streamer; meanwhile, the distorted electric field also speeds up the streamer velocity forward to both plates till bridging the anode and cathode plate; finally, the gas-gap is absolutely broken down.

Acknowledgements

This work was supported financially by National Natural Science Foundation of China, No. 51077032.

Conflicts of Interest

The authors declare no conflicts of interest regarding the publication of this paper.

References

- [1] Boris, J.P., Book, D.L. and Shasta, A. (1973) Fluid Transport Algorithm that Works. *Journal of Computational Physics*, **11**, 38-69. [https://doi.org/10.1016/0021-9991\(73\)90147-2](https://doi.org/10.1016/0021-9991(73)90147-2)
- [2] Zalesak, S.T. (1979) Fully Multidimensional Flux-Corrected Transport. *Journal of Computational Physics*, **31**, 335-362. [https://doi.org/10.1016/0021-9991\(79\)90051-2](https://doi.org/10.1016/0021-9991(79)90051-2)
- [3] Zheng, D.C. (2016) Numerical Simulation Methods for Gas Discharge. Science Press, Beijing.
- [4] Morrow, R. (1986) A Survey of the Electron and Ion Transport Properties of SF₆. *IEEE Transactions on Plasma Science*, **14**, 234-239. <https://doi.org/10.1109/TPS.1986.4316534>
- [5] Dhali, S.K. and Williams, P.F. (1987) Two-Dimensional Studies of Streamers in Gases. *Journal of Applied Physics*, **62**, 4696-4707. <https://doi.org/10.1063/1.339020>
- [6] Kulikovskiy, A.A. (1995) Two-Dimensional Simulation of the Positive Streamer in N₂ between Parallel-Plate Electrodes. *Journal of Physics D: Applied Physics*, **28**, 2483-2493. <https://doi.org/10.1088/0022-3727/28/12/015>
- [7] Georghiou, G.E., Morrow, R. and Metaxas, A.C. (1999) The Theory of Short Gap Breakdown of Needle Point-Plane Gaps in Air Using Finite-Difference and Finite-Element Methods. *Journal of Physics D: Applied Physics*, **32**, 1370-1385. <https://doi.org/10.1088/0022-3727/32/12/314>
- [8] Lehmann, K.K. and Callegari, C. (2002) Quantum Hydrodynamic Model for the Enhanced Moments of Inertia of Molecules in Helium Nanodroplets: Application to SF₆. *The Journal of Chemical Physics*, **117**, 1595-1603. <https://doi.org/10.1063/1.1486443>
- [9] Pancheshnyi, S.V. and Starikovskii, A.Yu. (2003) Two-Dimensional Numerical Modelling of the Cathode-Directed Streamer Development in a Long Gap at High Voltage. *Journal of Physics D: Applied Physics*, **36**, 2683-2691. <https://doi.org/10.1088/0022-3727/36/21/014>
- [10] Chen, X.F. (2010) The Streamer Discharge Analysis in N₂, SF₆ and Their Mixtures

under the Uniform Electric Field. Master Thesis, Harbin University of Science and Technology, Harbin.

- [11] Morrow, R. (1991) Theory of Positive Corona in SF₆ Due to a Voltage Impulse. *IEEE Trans on Plasma Science*, **19**, 86-94. <https://doi.org/10.1109/27.106801>
- [12] Morrow, R. (1987) Properties of Streamers and Streamer Channels in SF₆. *Physical Review A*, **35**, 1778. <https://doi.org/10.1103/PhysRevA.35.1778>
- [13] Zheng, D.C. (2019) SF₆ Dielectric Behaviors and Application. Science Press, Beijing.
- [14] Zhu, S.H. (2012) The Dynamic Behaviors of Discharge Process in SF₆/N₂ in Short-Gap. Master Thesis, Harbin University of Science and Technology, Harbin.
- [15] Boris, J.P. and Book, D.L. (1976) Solution of Continuity Equations by the Method of Flux-Corrected Transport. *Methods in Computational Physics*, **1**, 85-129. <https://doi.org/10.1016/B978-0-12-460816-0.50008-7>
- [16] Sato, N. (1980) Discharge Current Induced by the Motion of Charged Particles. *Journal of Physics D: Applied Physics*, **13**, 3-6. <https://doi.org/10.1088/0022-3727/13/1/002>
- [17] Boris, J.P. and Book, D.L. (1973) Flux-Corrected Transport. I. SHASTA, a Fluid Transport Algorithm That Works. *Journal of Computational Physics*, **11**, 38-69. [https://doi.org/10.1016/0021-9991\(73\)90147-2](https://doi.org/10.1016/0021-9991(73)90147-2)
- [18] Pedersen A. (1967) Calculation of Spark Breakdown or Corona Starting Voltages in Nonuniform Fields. *IEEE Transactions on Power Apparatus and Systems*, **PAS-86**, 200-206. <https://doi.org/10.1109/TPAS.1967.291836>
- [19] Luque, A. and Ratushnaya, V. (2008) Ute Ebert, Positive and Negative Streamers in Ambient Air: Modelling Evolution and Velocities. *Journal of Physics D: Applied Physics*, **41**, 1-18. <https://doi.org/10.1088/0022-3727/41/23/234005>
- [20] Raether, H. (1964) Electron Avalanches and Breakdown in Gases. Butterworths, London, 15-22.
- [21] Bonisch, S., Kalkner, W. and Pommerenke, D. (2003) Modeling of Short-Gap ESD under Consideration of Different Discharge Mechanisms. *IEEE Transactions on Plasma Science*, **31**, 736-744. <https://doi.org/10.1109/TPS.2003.815823>
- [22] Georghiou, G.E., Papadakis, A.P., Morrow, R. and Metaxas, A.C. (2005) Numerical Modelling of at Mospheric Pressure Gas Discharges Leading to Plasma Production. *Journal of Physics D: Applied Physics*, **38**, 303-328. <https://doi.org/10.1088/0022-3727/38/20/R01>
- [23] Pancheshnyi, S.V., Starikovskaia, S.M. and Starikovskii, A.Y. (2001) Role of Photoionization Processes in Propagation of Cathode-Directed Streamer. *Journal of Physics D: Applied Physics*, **34**, 1-11. <https://doi.org/10.1088/0022-3727/34/1/317>